Measurement of spatial stress gradients near grain boundaries

Basu, Indranil; Ocelík, Vaclav; De Hosson, Jeff Th M.

Published in:
Scripta Materialia

DOI:
10.1016/j.scriptamat.2017.03.036

Publication date:
2017

Measurement of spatial stress gradients near grain boundaries

I. Basu*, V. Ocelík, J.Th.M De Hosson

Department of Applied Physics, Zernike Institute for Advanced Materials and Materials innovation institute, University of Groningen, 9747AG Groningen, The Netherlands

*Corresponding author: **i.basu@rug.nl**

Abstract

A correlative method based on Electron Back Scattered Diffraction and Focused ion-beam – Digital image correlation slit milling technique was used to quantitatively determine spatially resolved stress profiles in the vicinity of grain boundaries in pure titanium. Measured local stress gradients were in good agreement with local average misorientation and experimentally calculated geometrically necessary dislocation densities. Stress profiles within few hundred to thousand nanometers near the grain boundary display a local minimum, followed by a typical Hall-Petch type variation of "one over square root of distance". The observed trends allude to local stress relaxation mechanisms active near grain boundaries.

The term "residual stress" prescribes to locked in stresses, which remain after materials processing. These stresses span across different length scales. The influence of microstructure i.e. spatial distribution of grains and phases, is significant on local residual stress distribution. In particular, grain boundaries contribute significantly to build up of such internal stresses, owing to varied mechanical response of different grain orientations during plastic deformation.

In metals, the motion and interaction of dislocations within the material microstructure and their resultant impact on micro scale plasticity is crucial for understanding the macroscopic mechanical performance and failure resistance of a component. Dislocations can not only interact among themselves but also with other crystal defects such as grain boundaries, often giving rise to complex geometrical configurations of stored dislocations that are associated with long-range elastic stress fields. Superposition of such stress fields invariably results in a strong spatial heterogeneity in local stress states, which directly determines preferential zones for damage nucleation and thereby fracture characteristics in materials.

Stored dislocations are generally classified into two types viz. geometrically necessary dislocations (GNDs) that accommodate a lattice curvature from a deformation gradient; and

statistically stored dislocations (SSDs), which accumulate due to statistical entanglements. While SSDs are prone to rearrangement by thermally activated processes such as cross-slip or climb, GNDs maintain the lattice continuity across multiple grains during plastic deformation, hence acting as the primary contributors to strain hardening. Needless to say the variation of local GND density levels directly influences the distribution of residual stresses in the interior of the grain. Such correlation between GND density levels and local stress gradients has been utilized in the past to explain local hardening phenomenon due to dislocation pile up at grain boundaries. Eshelby et al. [1] showed analytically that the dislocation pile up ahead an insurmountable obstacle such as grain boundary would result in a stress gradient that varies as 'one over square root' of the distance from the obstacle. Subsequent experimental observations by Hall [2,3] and Petch [4] independently re-established such a behavior in metals as the well-known Hall-Petch effect, wherein the mechanical strength of the material increases with decreasing grain size.

The dislocation configuration near a grain boundary strongly determines the degree of pile up and corresponding local stress concentration. Depending on the crystallography of the grain boundary certain slip systems may find conjugate systems in the neighboring grain that facilitate complete or partial slip transfer. A theoretical estimate of the feasibility of slip transmission can be described by the slip transfer parameter [5,6], expressed as $m' = (\boldsymbol{n_1} \cdot \boldsymbol{n_2}).(\boldsymbol{b_1} \cdot \boldsymbol{b_2})$, where $\boldsymbol{n_1}$ and $\boldsymbol{n_2}$ are the normalized intersection lines common to the slip planes and the boundary plane, and $\boldsymbol{b_1}$ and $\boldsymbol{b_2}$ are the normalized slip directions in the pile-up and emission grains. The value of m' provides a measure of the probability for possible transmissivity of a dislocation across the grain boundary. Maximization of slip transfer parameter m' abates dislocation pile up and promotes easier slip transfer across the grain boundary.

Quantitative measurement of spatially dependent local stress states near grain boundaries therefore becomes crucial in understanding fracture mechanisms in structural materials. Spatially resolved internal stress measurements can be made using high resolution electron back scatter diffraction (HR-EBSD) wherein Kikuchi patterns from reference (un-deformed) and deformed states are cross-correlated to measure the residual elastic strains, and subsequently calculate the local elastic stress state [7,8]. However, the method is limited to 2-dimensional investigations wherein only surface information is obtained [9]. On the other hand, residual stress measurements using focused ion beam – digital image correlation (FIB–DIC) technique allows

simultaneous sub-micron lateral and depth resolution in a semi-automated and robust way [10], thereby accounting for both surface and bulk deformation contribution on internal stress build up.

The novelty of the current work lies in introducing a site specific method utilizing electron back scattered diffraction (EBSD) and FIB-DIC slit milling to accurately determine spatially resolved stress profiles in the vicinity of grain boundaries in commercially pure titanium. Correlations with the GND dislocation density and slip transfer parameter are drawn to validate the stress measurements. The observed trends are subsequently discussed with respect to underlying physical processes and its subsequent impact on fracture resistance of titanium is acknowledged.

Commercially available grade II titanium was subjected to room temperature in-situ four point bending test inside a Tescan Lyra dual beam (FEG-SEM/FIB) scanning electron microscope. Prior to mechanical testing, bending specimens were prepared for EBSD measurements using conventional metallographic techniques [11]. Specimens were strained to a final surface true strain, $\varepsilon = 0.05$. Microstructural characterization was performed by means of EBSD, thereby extracting both topographical and orientation information of individual grains. A step size of 0.3 μm and hexagonal type of grid was used for the measurements. The step size is optimized such that both the dislocation density averaging that increases with step size and interference from EBSD measurement noise (decreasing with increasing step width) are minimized [12]. The acquired raw EBSD data was subsequently analyzed using EDAX-TSL OIM^{TM} Analysis 7 software and MTEX Matlab toolbox [13]. Slip traces in individual grains were imaged using in-situ scanning electron microscopy (SEM). The orientation of the grain boundary plane was determined by milling into the region containing the boundary using focused ion beam and examining the grain boundary trace along the milled cross section. All observations were made on the tensile surface of the bent specimen, with the direction of viewing parallel to the surface normal, hereinafter referred to as *A3* sample axis.

Local stresses near grain boundaries were experimentally determined by the FIB-DIC slit milling technique [14]. The method relies on the measurement of displacements induced due to stress relaxation in the vicinity of the milled slit. The stress relaxation is owing to local removal of material, thereby creating two traction free surfaces. Displacements can be either towards the slit centerline indicating a residual compressive stress or away from the slit (residual tensile stress).

The measured values are correspondingly fitted to an analytical expression describing internal stress as a function of displacements normal to slit length. For more details of the technique and analysis the reader is referred to [15]. In this contribution we concentrate on the materials physics aspects and to the structure-property relationship in metallic systems. Linear slits, oriented normal to the grain boundary trace, of a fixed width 0.5 μm, depth 2.5 μm, and lengths varying from 15-25 μm (depending on the grain size), were milled inside individual grains showing pile up as per local misorientation data. Measurements were performed on multiple grains showing different degrees of pile up. For each slit, multiple SEM images of resolution 768x768 pixels were acquired at high magnifications (field of view of 10 – 15 μm) to ensure a high spatial resolution of measured displacement field. DIC was performed using commercial software GOM Correlate 2016. Facet size of 19 x 19 pixels with a step width of 16 pixels was chosen in order to obtain statistically sufficient data points. Yttria-stabilized Zirconia (YSZ) nano-particles were used for surface decoration to obtain optimum image contrast for high accuracy DIC analysis. It must be noted that though the YSZ nano-particles are able to provide a sharply defined surface decoration over reasonably large surface areas, the particle size distribution may be locally inhomogeneous [16]. Unsolved facets due to such local heterogeneity in the particle sizes, were omitted from the calculations.

Stress distribution at sub-microscopic length scales need not always be homogeneous i.e. constant stress all throughout the material, but may considerably vary spatially. In such cases, stress determination by simplistic averaging of all displacements along the slit length i.e. singular fitting (c.f. Supplementary Fig. S1a), misrepresents the actual stress state of the material. Supplementary Figs. S2a and S2b illustrate examples of homogeneous and heterogeneous displacements. A multiple fitting approach as described in reference [15], wherein a stress value corresponding to each row of displacements is obtained (c.f. Supplementary Fig. S1b), was implemented to account for spatially heterogeneity in stresses along the slit length. Supplementary Fig. S1c shows the corresponding deviation between the stress values measured by multiple fitting approach in comparison with that obtained from singular fitting (one stress value for the whole slit). In order to simplify calculations, an isotropic elastic modulus tensor was assumed for stress determination from the measured displacements.

Figure 1 (a) KAM and (b) Grain orientation maps for *Grain 2* and its neighborhood; (c) GND density and LAM profile between points A and B

Figure 1 illustrates a representative case of a grain associated with a strong pile up, labelled as *Grain 2*. Figs. 1a and 1b represent the Kernel Average Misorientation (KAM) and the grain orientation maps respectively. The KAM physically describes the average misorientation spread between a reference pixel and its nearest neighbor pixels for a defined kernel size. KAM values were calculated for the 2nd nearest neighbor with a threshold value of 2° [17]. High angle grain boundaries, classified as larger than 15°, are highlighted in white in Fig. 1a. The KAM value indicates a strong pile up at the grain boundary separating *Grain 1* and *Grain 2*. The grain orientations in Fig. 1b are depicted in unit cell representation with inverse pole figure color coding. The viewing axis corresponds to the *A3* direction. The grain boundaries in Fig. 1b are additionally colored with respect to their respective slip transfer parameter value that ranges from dark blue corresponding to no slip transfer to light yellow indicating complete transmissivity. The grain boundary segment between *Grain 1* and *Grain 2* displays a low probability of slip transfer, with an m' value between 0.3 and 0.4. Fig. 1c shows the variation of local average misorientation (LAM) and GND density with respect to distance from the grain boundary (refer to highlighted line AB in Fig. 1a). The LAM angle corresponds to the misorientation averaged over all nearest neighbor pairs within a kernel. GND density (ρ_{GND}) values from EBSD data were calculated using the strain gradient approach [18,19], given by the expression: $\rho_{GND} = \frac{2\theta}{na|\boldsymbol{b_d}|}$, where θ is the experimentally measured KAM value, a is the step size, n is the number of nearest neighbors averaged in the KAM calculation and $\boldsymbol{b_d}$ is the Burgers vector corresponding to the active slip system in the grain. The excellent agreement between the LAM and GND values is unsurprising since both values are derived from local misorientation. Interestingly both trends reveal a local minimum close to the grain boundary highlighted by the shaded region in Fig. 1c.

Figure 2 (a) SEM image showing slit and (b) grain boundary plane orientation; (c) measured stress profile between points A and B

Figure 2 represents the FIB-DIC analysis and corresponding stress measurements for the region shown in Fig. 1. Fig. 2a shows the spatial orientation of the milled slit with respect to the grain boundary. The white dots correspond to the YSZ particles used for surface decoration. *Grain 2* shows profuse slip bands that were identified as $(10\bar{1}0)$ prismatic plane traces. Fig. 2b represents the orientation of the grain boundary plane with respect to the slit direction represented by the red arrow, indicating that longitudinal direction of slit is parallel to the grain

boundary normal within the measurement volume. Fig. 2c displays the measured stress profile as a function of normal distance from the grain boundary. The measured stress component σ_{12} describes the stress acting parallel to the grain boundary plane and perpendicular to the length of the slit. The stress values within a distance of 1.3 μm from the grain boundary show a local minimum, which is succeeded by a stress peak that monotonically decreases with increasing distance from the grain boundary. On comparing the stress gradient with Fig. 1c the agreement seems excellent, thereby indicating that the observed stress fluctuations indeed confer to the actual stress state near the grain boundary. The data points corresponding to distances greater than 1.3 μm show a good fit to the theoretically known 'one over square root of distance' Hall-Petch variation [2–4](c.f. Fig. 2c). It is worthwhile to note that the stress profile is tensile in nature near the grain boundaries with gradual transition into compressive stresses in the grain interior. The Hall-Petch coefficient k_{HP} corresponding to *grain 2* is empirically determined to be 1.047 MPa.m$^{0.5}$.

The initial stress minimum observed in Fig. 2c indicates activation of local stress relaxation mechanisms, wherein dislocation spacing seems to equilibrate in regions very close to the boundary i.e. pile up effect is abated locally. Slip trace analysis inside *Grain 2* revealed activation of more than one prismatic slip systems near the grain boundary (most likely nucleating at the grain boundary due to stress fields exerted by the neighboring grain), whereas singular slip took place in the grain interior (c.f. Figs. 2a and 3a). The observed orientation gradients and lattice rotation about the c-axes shown in Fig. 3a further indicate relatively more intense slip activity in the vicinity of the grain boundary as compared to the grain interior. An easier dislocation generation, along with activation of more than one deformation modes, would locally enhance dislocation – dislocation interactions close to the boundary i.e. passing and cutting stresses, which can significantly retard dislocation motion in the region.

Another contributing factor could be the change in the local stress state very close to the grain boundary that may lead to spatial delocalization of dislocation cores at the tip of the pile up, thereby locally depleting the dislocation density ahead of the pile up. During plastic deformation, lattice dislocation segments trapped by the grain boundary may overlap with dislocation cores of grain boundary dislocations (GBDs), giving rise to *non-equilibrium grain boundary* configurations. The resultant elastic stress fields generated from such interactions are long

ranged in nature and can become sufficiently high to influence dislocation slip in a rather thick grain boundary mantle [20–22]. The observed spread in the KAM values (c.f. Fig. 1a) along the grain boundary for *Grain 2* most likely results from such local spreading of dislocations at the tip of pile ups, originating from multiple slip-grain boundary intersection sites.

Figure 3 (a) SEM image of prismatic slip traces, inverse pole figure map and unit cells depicting slip induced lattice rotation near the grain boundary; (b) variation of k_{HP} and relaxation width with the peak GND density for each grain

Since the local residual stresses determined post plastic deformation are directly linked to the magnitude of elastic stresses exerted by the (edge) dislocations present in that region, the observed stress relaxation near the grain boundary is attributed to relative decrement in the dislocation density levels at the grain boundary. Fig. 3b shows the variation of Hall-Petch coefficient k_{HP} and the width of the relaxed volume as a function of the peak value of GND density for different grains. The results indicate that both the width of volume experiencing stress relaxation in a grain as well as the Hall-Petch coefficient k_{HP} increases with higher GND density levels. The trends also reveal that for higher k_{HP} values the width of the zone near the grain boundary showing stress minimum increases. The Hall-Petch coefficient, also called the *dislocation locking parameter*, typically describes the resistance to slip nucleation or transfer in the neighboring grain [23]. In other words larger the value of k_{HP}, more and more lattice dislocation segments will be absorbed by the grain boundary i.e. higher trapped lattice dislocation (TLDs) densities. Since the elastic stress field from the interaction between TLDs and GBDs varies linearly with $\sqrt{\rho_{TLD}(m^{-1})}$, higher TLD densities (ρ_{TLD}) would subsequently lead to aforementioned delocalization effects over a wider zone adjacent to the grain boundary [22]. For instance, assuming a ρ_{TLD} in the range of $10^8 m^{-1}$, non-equilibrium grain boundary stress fields can be of the order of $10^{-3}G$ even at distances $\approx 10^4 . b_d$ (where, G is the shear modulus and b_d is the Burgers vector for active dislocation slip) from the grain boundary plane. Also noteworthy is the significant scatter seen in the k_{HP} values for different grains (c.f. Fig. 3b), compared to the average Hall-Petch coefficient for polycrystal Ti of $0.4 MPa.m^{0.5}$ [24]. The large fluctuations in Hall–Petch coefficients suggest its strong dependence upon the local grain orientation and grain boundary geometry.

The implications of the observations in the current work are significant in terms of understanding fracture resistance in titanium. The measured stress profile in Fig. 2c indicates a transition from

tensile to compressive stress state on moving away from the boundary. A tensile stress state at the grain boundary would promote fracture by crack nucleation [25] and hence highlights the detrimental role of grain boundaries in fracture resistance. However, the observed stress relaxation in the vicinity of the grain boundary sheds light on locally active intrinsic mechanisms that may aid in delaying damage nucleation at grain boundaries.

A novel correlative technique utilizing EBSD and FIB-DIC method for obtaining site specific microstructural and local stress information is presented. Stress gradients due to dislocation pile up at pure titanium grain boundaries are quantified. The following conclusions are drawn:

1. Stored dislocation densities and stress values near the grain boundary revealed a local minimum, deviating from the expected Hall-Petch characteristics.
2. The observed stress drop is justified by a local change in elastic stress fields arising from dislocation-dislocation and dislocation-grain boundary interactions that lead to a relative depletion of dislocation densities in the vicinity of the boundary
3. The k_{HP} values measured for different grains ranged from $0.14\ MPa.m^{0.5}$ to $1.047\ MPa.m^{0.5}$, indicating a strong dependence of the local strengthening behavior on the grain orientation and grain boundary crystallography. The width of the zone undergoing stress relaxation near a grain boundary scales non-linearly with increasing value of k_{HP} and peak dislocation densities, varying from $500\ nm$ to $1300\ nm$.
4. The observations in the current work have significant implications on the generic understanding of grain boundary damage mechanisms.

Acknowledgement

This research was carried out under project number T61.1.14545 in the framework of the Research Program of the Materials innovation institute (M2i) (www.m2i.nl). IB would like to thank Herman Fidder for providing titanium material.

References

[1] J.D. Eshelby, F.C. Frank, F.R.N. Nabarro, Lond. Edinb. Dublin Philos. Mag. J. Sci. 42 (1951) 351–364.
[2] E.O. Hall, Proc. Phys. Soc. Sect. B 64 (1951) 747.
[3] E.O. Hall, Nature 173 (1954) 948–949.
[4] N.J. Petch, J Iron Steel Inst 174 (1953) 25–28.
[5] Z. Shen, R.H. Wagoner, W.A.T. Clark, Acta Metall. 36 (1988) 3231–3242.
[6] W.A.T. Clark, R.H. Wagoner, Z.Y. Shen, T.C. Lee, I.M. Robertson, H.K. Birnbaum, Scr. Metall. Mater. 26 (1992) 203–206.

[7] T.B. Britton, A.J. Wilkinson, Ultramicroscopy 111 (2011) 1395–1404.
[8] T. Benjamin Britton, A.J. Wilkinson, Acta Mater. 60 (2012) 5773–5782.
[9] Y. Guo, D.M. Collins, E. Tarleton, F. Hofmann, J. Tischler, W. Liu, R. Xu, A.J. Wilkinson, T.B. Britton, Acta Mater. 96 (2015) 229–236.
[10] B. Winiarski, P.J. Withers, J. Strain Anal. Eng. Des. 50 (2015) 412–425.
[11] B. Taylor, E. Weidmann, Struers Den. Rosendahls Bogtryk (2008).
[12] J. Jiang, T.B. Britton, A.J. Wilkinson, Ultramicroscopy 125 (2013) 1–9.
[13] R. Hielscher, H. Schaeben, J. Appl. Crystallogr. 41 (2008) 1024–1037.
[14] K.J. Kang, N. Yao, M.Y. He, A.G. Evans, Thin Solid Films 443 (2003) 71–77.
[15] C. Mansilla, D. Martínez-Martínez, V. Ocelík, J.T.M. De Hosson, J. Mater. Sci. 50 (2015) 3646–3655.
[16] B. Winiarski, G.S. Schajer, P.J. Withers, Exp. Mech. 52 (2012) 793–804.
[17] M. Calcagnotto, D. Ponge, E. Demir, D. Raabe, Mater. Sci. Eng. A 527 (2010) 2738–2746.
[18] L.P. Kubin, A. Mortensen, Scr. Mater. 48 (2003) 119–125.
[19] P.J. Konijnenberg, S. Zaefferer, D. Raabe, Acta Mater. 99 (2015) 402–414.
[20] M.W. Grabski, R. Korski, Philos. Mag. 22 (1970) 707–715.
[21] R.C. Pond, D.A. Smith, Philos. Mag. 36 (1977) 353–366.
[22] A.A. Nazarov, A.E. Romanov, R.Z. Valiev, Acta Metall. Mater. 41 (1993) 1033–1040.
[23] R. Armstrong, I. Codd, R.M. Douthwaite, N.J. Petch, Philos. Mag. 7 (1962) 45–58.
[24] G. Gottstein, Physical Foundations of Materials Science, Springer Science & Business Media, 2013.
[25] G. Irwin, J Appl Mech (1957).

Figure 1

Click here to download high resolution image

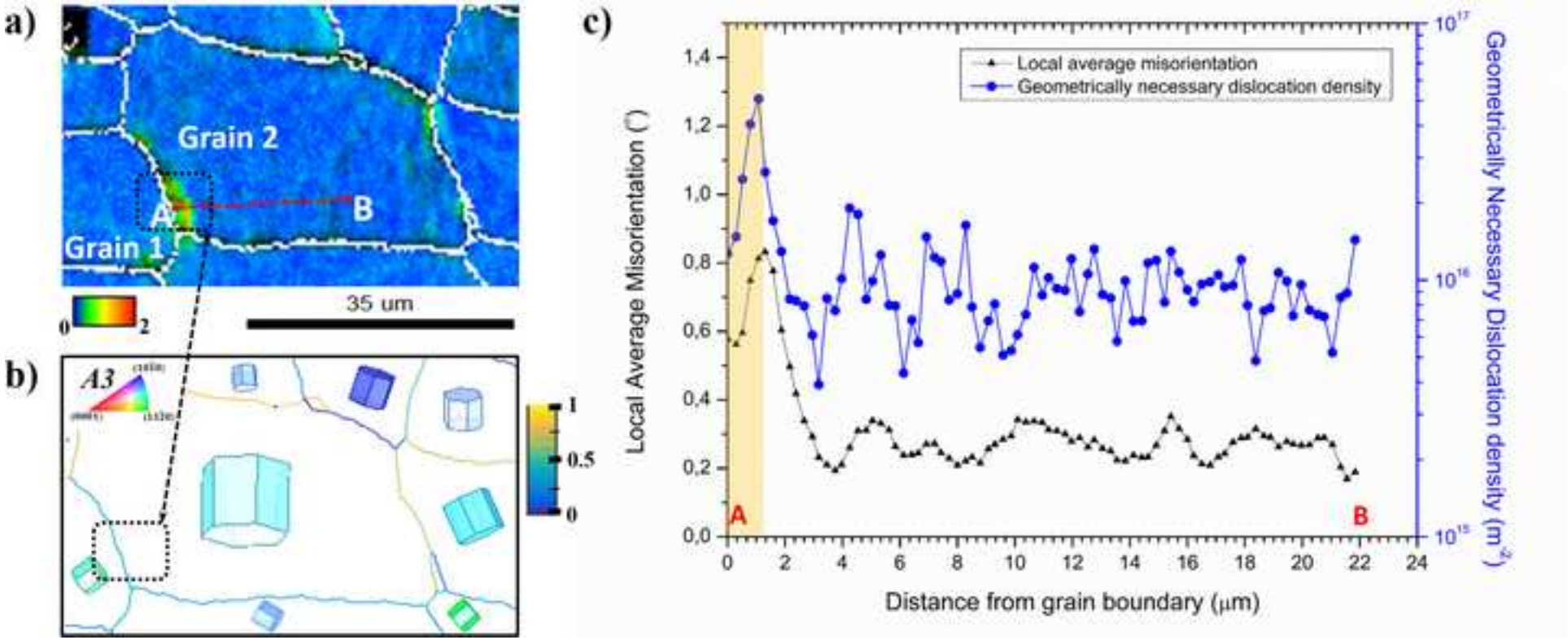

Figure 2

Click here to download high resolution image

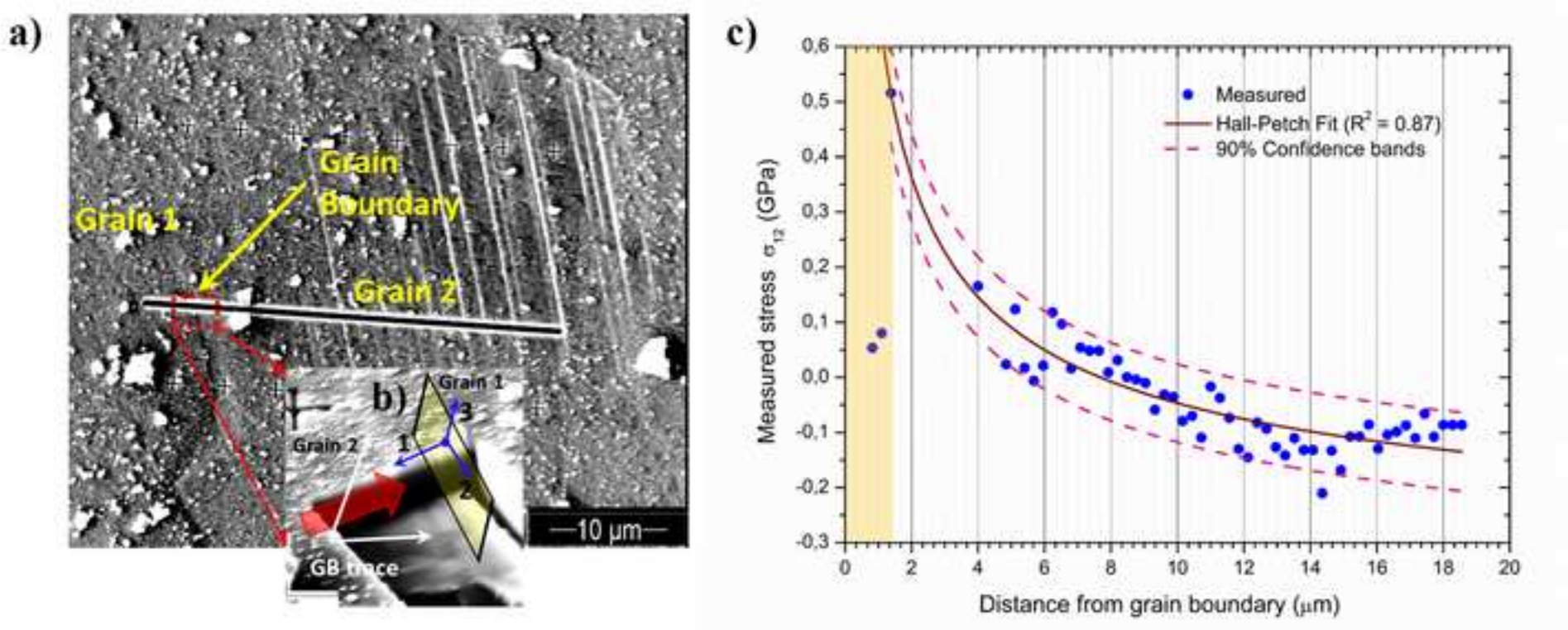

Figure 3

Click here to download high resolution image

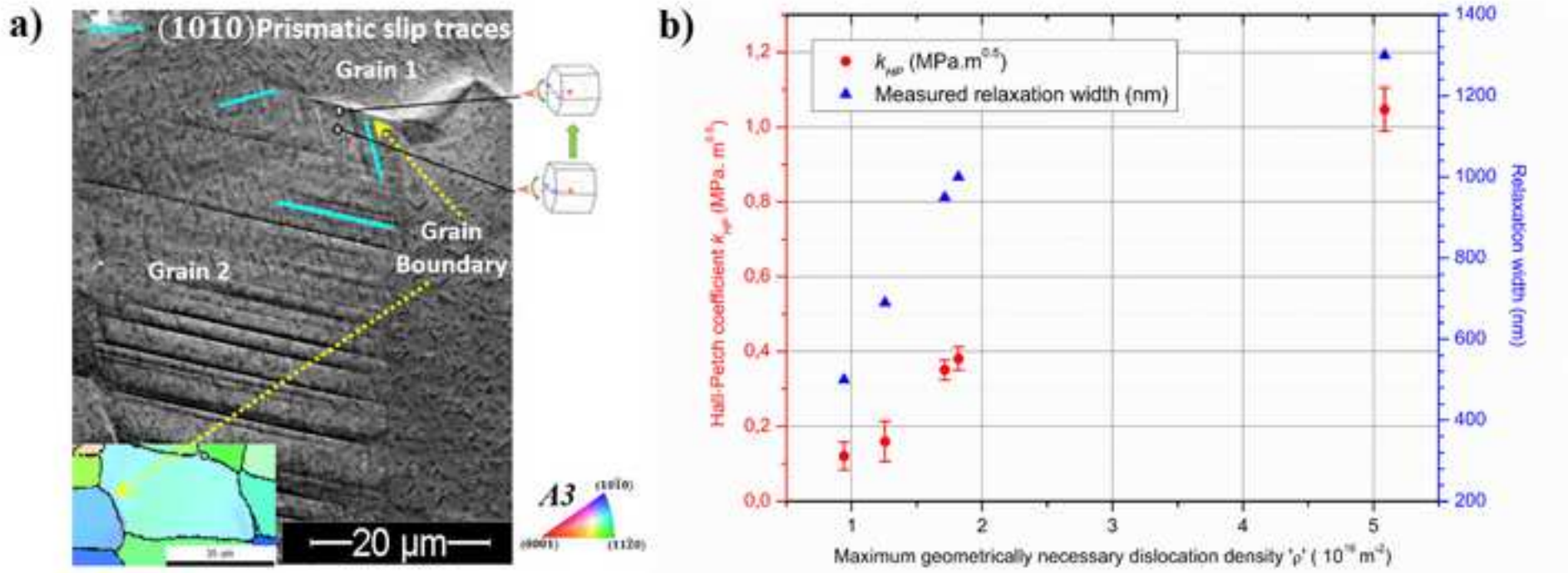

Appendix A: Supplementary Figures

Click here to download Supplementary Material: Supplementary Figures.pdf